Published in final edited form as:

Nat Chem Biol. 2017 October ; 13(10): 1096–1101. doi:10.1038/nchembio.2456.

Optogenetic control of kinetochore function

Huaiying Zhang[1,+], **Chanat Aonbangkhen**[2,+], **Ekaterina V. Tarasovetc**[1], **Edward R. Ballister**[1], **David M. Chenoweth**[2,*], and **Michael A. Lampson**[1,*]

[1]Department of Biology, School of Arts and Sciences, University of Pennsylvania, Philadelphia, Pennsylvania 19104, USA

[2]Department of Chemistry, School of Arts and Sciences, University of Pennsylvania, Philadelphia, Pennsylvania 19104, USA

Abstract

Kinetochores act as hubs for multiple activities during cell division, including microtubule interactions and spindle checkpoint signaling. Each kinetochore can act autonomously, and activities change rapidly as proteins are recruited to or removed from kinetochores. Understanding this dynamic system requires tools that can manipulate kinetochores on biologically relevant temporal and spatial scales. Optogenetic approaches have the potential to provide temporal and spatial control with molecular specificity. Here we report new chemical inducers of protein dimerization that allow us to both recruit proteins to and release them from kinetochores using light. We use these dimerizers to manipulate checkpoint signaling and molecular motor activity. Our findings demonstrate specialized properties of the CENP-E (kinesin-7) motor for directional chromosome transport to the spindle equator and for maintaining metaphase alignment. This work establishes a foundation for optogenetic control of kinetochore function, which is broadly applicable to experimentally probe other dynamic cellular processes.

Introduction

The kinetochore is a complex macromolecular structure, comprised of more than 100 different proteins, that assembles at the centromere of each chromosome during cell division[1,2]. Kinetochores perform multiple essential tasks for chromosome segregation, including building physical connections between chromatin and the force generating microtubule (MT) polymers, and housing regulatory proteins that ensure faithful segregation[3]. Defects in these processes lead to chromosome segregation errors and genome

*Corresponding authors: M.A.L. (lampson@sas.upenn.edu), D.M.C. (dcheno@sas.upenn.edu).
+Equal contribution

Author Contributions

H.Z. designed and conducted biological experiments and wrote the manuscript. C.A. synthesized and characterized the dimerizers, conducted experiments in Figure 1, Supplementary Figure 1, 2 and edited the manuscript. E.V.T. conducted experiments in Figure 4 and Supplementary Figure 4. E.R.B. contributed to the design of dimerizers and checkpoint experiments. D.M.C. and M.A.L. designed experiments and edited the manuscript.

Competing Financial Interests Statement

We claim no competing financial interests.

instability, which are associated with cancer and developmental diseases[4]. Kinetochore function depends on dynamic localization changes of components such as kinases, molecular motors and mitotic checkpoint proteins. For example, coordinated actions of plus and minus-end directed MT motors drive chromosome movements to align at the spindle equator[5,6] (Figure 1a). This process of chromosome congression facilitates attachment of sister kinetochores to opposite spindle poles (bi-orientation), so that each daughter cell ultimately receives exactly one copy of each chromosome. Dynein initially transports chromosomes towards MT minus-ends at spindle poles, and then a kinesin-7 motor, CENP-E, transports them to MT plus-ends at the spindle equator (Figure 1a). The spindle checkpoint provides sufficient time for all chromosomes to congress and bi-orient by delaying anaphase in the presence of kinetochores lacking proper MT attachment[7,8]. Checkpoint signaling proteins are enriched on unattached kinetochores to activate the checkpoint and released from attached kinetochores to silence the checkpoint (Figure 1a). Each kinetochore can act autonomously, so that a single unattached kinetochore can signal the whole cell to wait before proceeding to anaphase. After congression and bi-orientation, kinetochores maintain stable attachments to dynamic microtubule plus-ends, which will ultimately drive chromosome segregation in anaphase (Figure 1a).

A promising approach for understanding this complex and dynamic system is to manipulate kinetochores on biologically relevant temporal and spatial scales, with molecular specificity, which has not been possible with existing methods. Molecular approaches such as genetic manipulations or RNA interference (RNAi) target specific proteins[9] but lack spatial and temporal control. Small-molecule inhibitors offer temporal, but not spatial control, and their molecular specificity is variable and difficult to thoroughly characterize[10]. Laser microsurgery can be used to ablate single kinetochores with temporal control but lacks molecular specificity[11].

Optogenetic tools have the potential to provide both spatiotemporal control using light and molecular specificity by using genetically encoded protein tags, and have emerged as important tools to probe dynamic cellular processes such as organelle transport, cell signaling and polarity[12–14]. We previously reported a photocaged chemical dimerizer that can recruit tagged proteins from the cytosol to multiple cellular structures[15,16]. Using this molecule, dimerization can be reversed by adding a competitor, but a major limitation is that reversal is slow and lacks spatial control. One feature of this system is the modular design of the dimerizer, which facilitates the development of new molecules on the same platform.

Here we exploit this design by developing two new dimerizers. One can be uncaged with less light and longer wavelengths. The other allows reversal of dimerization so that proteins can be recruited to and subsequently released from cellular structures. We apply those dimerizers to manipulate two important kinetochore functions: checkpoint signaling and molecular motor activity. Overall, our findings establish a foundation for opotogenetic manipulation of kinetochores and reveal specialized properties of the motor protein CENP-E for transporting chromosomes specifically towards the spindle equator and for stabilizing the metaphase plate.

Results

New optogenetic tools

Our previously reported dimerizer (NTH) (**1**) contains three modules: a 6-nitroveratryl oxycarbonyl (NVOC) photocage to prevent untargeted dimerization, trimethoprim (TMP) that non-covalently binds to *Escherichia coli* dihydrofolate reductase (eDHFR), and Haloligand that covalently binds to a bacterial alkyldehalogenase enzyme (referred to as Haloenzyme, Figure 1b). Illumination removes the photocage, allowing dimerization of eDHFR-tagged proteins with Halo-tagged proteins. Based on this modular design, we developed two new dimerizers that offer additional properties: increased sensitivity to light and rapid light-induced reversal of dimerization.

First, we replaced the NVOC with a [7-(diethylamino)-coumarin-4-yl]methyl (DEACM) photocage, which is more sensitive to light and can be uncaged at longer wavelengths[17]. Details of the synthetic scheme and characterization can be found in supplementary information. This new molecule (CTH (**2**), Figure 1b) enters living cells, as shown with cells expressing Haloenzyme fused to the centromere protein CENP-B (Supplementary Results, Supplementary Figure 1a), and is not toxic to cells at concentrations used in our experiments (Supplementary Figure 1b). To show that CTH can recruit proteins from the cytosol to cellular structures, we targeted mCherry to mitochondria by uncaging CTH with 385 nm light. Notably, CTH requires less light than NTH to uncage (Figure 1c), and CTH can be uncaged with 444 nm light whereas NTH is only sensitive to shorter wavelengths (Supplementary Figure 1c, d).

Second, we developed a dimerizer that can be cleaved with light to reverse dimerization. Taking advantage of the modular design of our system, we inserted a cleavable NVOC linker in between the Halo and TMP ligands to make TNH (**3**) (Figure 1b). Details of the synthetic scheme and characterization can be found in Supplementary Note. To show that TNH enters live cells and recruits proteins to cellular structures, we targeted mCherry-eDHFR to mitochondria. The kinetics of recruitment depend on TNH concentration (Supplementary Figure 1e), with the highest degree of dimerization ($t_{1/2}$ ~2 minutes) observed at 0.1 μM. A higher concentration (1 μM) is less effective because independent occupancy of both protein binding sites with two different TNH molecules would lead to unproductive protein-ligand complexes. A lower concentration (0.01 μM) required more time ($t_{1/2}$ ~5 minutes) to achieve maximum dimerization (~80% of that at 0.1 μM). TNH is not toxic to cells at these concentrations (Supplementary Figure 1b). To test whether the recruitment can be reversed with light, we targeted multiple regions sequentially with a 405 nm laser (Figure 1d). mCherry was released rapidly in the illuminated regions, demonstrating reversal of dimerization with spatiotemporal control.

As a functional test of the new dimerizers, we used them to control organelle transport. We previously showed that recruitment of kinesin or dynein motors to peroxisomes induces transport to the periphery or center of the cell, respectively[16]. Recruiting the dynein adapter BICD to peroxisomes by uncaging CTH led to peroxisome accumulation at the cell center, as expected (Supplementary Figure 2). To show that this transport can be halted by reversing dimerization, we used TNH to recruit an N-terminal fragment of kinesin light chain 1

(KLC1) to peroxisomes and subsequently cleaved it with light on one side of the cell (Figure 1e, yellow region). After incubation with TNH but before cleavage, peroxisomes were partially depleted from the interior of the cell. After illumination, peroxisomes remained on the cleaved side but depletion continued on the uncleaved side. Furthermore, peroxisomes accumulated in peripheral regions, where MT plus-ends are located, on the uncleaved side, as expected for kinesin-mediated transport (Figure 1e, f)[16]. These results demonstrate that organelle transport induced by dimerization can be arrested with spatial and temporal control by photocleaving the dimerizer.

Activating and silencing the spindle checkpoint

To test our ability to manipulate kinetochores, we first focused on the spindle checkpoint. The checkpoint is initially active when checkpoint proteins localize to kinetochores early in mitosis and then silenced when these proteins are removed from all kinetochores at metaphase, leading to anaphase onset. With TNH, we aimed to control both checkpoint activation and silencing by manipulating kinetochore localization of the checkpoint protein Mad1 (Figure 2a). For these experiments we used cells expressing eDHFR-mCherry-Mad1 together with Mis12-GFP-Halo or Halo-GFP-CENP-T, both constitutive kinetochore proteins. After adding TNH, Mad1 was recruited from the cytosol to metaphase kinetochores, and the spindle checkpoint was re-activated as <10% of cells proceeded to anaphase within 30 minutes. In comparison, >80% of control cells, which either did not express eDHFR-mCherry-Mad1 or were not treated with TNH, entered anaphase (Figure 2b, c, f). This re-activation is consistent with previous observations using rapamycin-induced dimerization[18,19]. Rapamycin is irreversible on the relevant time scale, but by cleaving TNH we could release Mad1 from kinetochores with light. Mad1 was undetectable at kinetochores after irradiation with 405 nm light, and >80% of cells proceeded to anaphase within 30 minutes (Figure 2d, f). To show spatial control, we released Mad1 from most but not all of the metaphase kinetochores, and cells remained arrested in metaphase (Figure 2e, f), indicating that Mad1 localization to a few kinetochores is sufficient for checkpoint activity. Together these results demonstrate control of both checkpoint activation and silencing.

CENP-E Transports chromosomes to the spindle equator

During chromosome congression, kinetochores that initially make lateral attachments to MTs are transported to the spindle poles by cytoplasmic dynein, a minus end-directed motor. The plus-end-directed kinetochore motor CENP-E then transports those chromosomes from the poles to the equator[20]. Successful congression depends on CENP-E transporting chromosomes selectively towards the plus-ends of spindle MTs facing the equator, but not towards the plus-ends of astral MTs facing the cortex, whereas polar ejection forces transport chromosomes in random directions[21]. To determine if this directional preference is a special property of CENP-E, we tested whether a plus-end directed motor which is not normally found at kinetochores, kinesin-1, can selectively transport chromosomes from poles to the equator (Figure 3a). For this experiment we used cells expressing Halo-GFP-SPC25, a constitutive kinetochore protein, together with K560-mCherry-eDHFR, the constitutively active motor domain of kinesin-1 as used previously[16]. We treated cells with a small molecule CENP-E inhibitor, GSK923295, which results in accumulation of some chromosomes at the poles[22], and then recruited kinesin-1 to kinetochores by uncaging CTH

at one pole (Figure 3b, yellow region). Chromosomes moved away from this pole while chromosomes at the unilluminated pole, serving as an internal control, showed little directional movement. The dynein/dynactin complex remains on kinetochores after kinesin-1 recruitment, indicating that the observed movement is not due to loss of dynein (Supplementary Figure 3). Because kinetochore-bound Halo-GFP-SPC25 exchanges with the cytoplasmic pool, kinesin-1 recruited to kinetochores at the uncaged pole gradually spread to other kinetochores that were not initially targeted, leading to small displacements of those kinetochores at longer time points. Nevertheless, it is clear that kinesin-1 transported chromosomes in all directions, without preference for MTs directed towards the metaphase plate (Figure 3c, d, e).

To test whether CENP-E selectively transports chromosomes from poles to the equator in this assay, we recruited the CENP-E motor domain rather than kinesin-1. Because the CENP-E inhibitor would prevent activity of the recruited CENP-E motors, we knocked down endogenous CENP-E with small interfering RNA (siRNA) that does not target our recruited motors. We designed two truncated CENP-E constructs which include the motor domain and parts of the coiled-coil domain (1–467 and 1–620 aa). Because these constructs lack the kinetochore binding site, they were freely diffusing in the cytosol before recruitment, and some chromosomes accumulated at the spindle poles as with the CENP-E inhibitor. After recruitment to kinetochores, either CENP-E construct transported chromosomes predominantly from the poles to the equator (Figure 4a–f). In contrast, kinesin-1 transported chromosomes equally in all directions (Supplementary Figure 4), as in our previous experiment with the CENP-E inhibitor (Figure 3). These results demonstrate that directional congression is a specialized property of CENP-E.

CENP-E maintains chromosomes at the metaphase plate

After transporting chromosomes to the equator, CENP-E remains at kinetochores, suggesting an additional role at bi-oriented kinetochores[23]. Indeed, after CENP-E deletion or depletion, bi-oriented kinetochores bind only half the normal number of MTs, and kinetochores are more frequently attached laterally rather than end-on to MTs[24,25]. In addition, CENP-E inhibition at metaphase with GSK923295 leads to chromosome movement towards the poles, which may reflect transport by poleward MT flux because the inhibitor generates a rigor state in which CENP-E is bound to the MT but inactive[22,26]. In vitro, CENP-E converts from a lateral transporter into a MT tip-tracker after reaching the MT end and maintains association with both assembling and disassembling MT tips[26]. If the tip-tracking activity contributes to CENP-E function in vivo, we predict that CENP-E would stabilize attachments between kinetochores and dynamic MT ends to maintain chromosome alignment at metaphase. To test this prediction, we established an assay to probe the stability of metaphase alignment by recruiting kinesin-1 to kinetochores to generate directional forces (Figure 5a). After recruiting kinesin-1 to metaphase kinetochores, the metaphase plate is mildly disturbed as the average distance of kinetochores to the equator increased slightly over time, compared to a stable metaphase plate in control experiment where no motor was recruited (Figure 5b–d). CENP-E inhibition generates some polar chromosomes, but those aligned at the metaphase plate maintain their positions over the time course of our experiment (10 minutes). In contrast, after recruiting kinesin-1 to kinetochores under CENP-

E inhibition, chromosomes at the metaphase plate rapidly lost alignment as the average distance of kinetochores to the equator increased dramatically (Figure 5b–d). This result indicates that after inhibiting CENP-E, the metaphase plate is less stable and therefore more prone to disruption by forces generated by recruited motors.

Discussion

We developed new optogenetic tools and applied them to control important kinetochore functions: spindle checkpoint signaling and motor activity. The first new molecule, CTH, has a red-shifted photocage, expanding the range of wavelengths that can be used for uncaging, and requires less light to uncage compared to our previously reported NTH. The second new molecule, TNH, offers spatiotemporal control over reversal of dimerization. Our system has both advantages and disadvantages compared to photosensitive protein dimerization systems. For example, the TULIP system does not provide controlled reversibility, but rather relies on the dissociation kinetics of the protein-protein interaction[27]. The phytochrome B – phytochrome-interacting factor system can be switched on and off repeatedly using different wavelengths of light, but was not successful in targeting kinetochores[28,29]. With our system, light can be used to either trigger dimerization or to reverse dimerization, depending on the choice of dimerizer, but not for repeated ON/OFF cycles. The modular design supports further expansion, however, through creation of new dimerizers with additional properties. For example, a future goal is to combine the orthogonal coumarin photocage and NVOC linker to create a molecule that allows spatiotemporal control for both dimerization and reversal of dimerization.

Previous experiments targeting Mad1 to kinetochores showed that the checkpoint is activated by constitutive tethering or by rapamycin-induced recruitment[18,19,30], but the effects of removing Mad1 could not be examined because the targeting was not reversible. Our results show that cells progress to anaphase after removal of Mad1 from kinetochores by TNH cleavage, thus providing control over cell cycle progression through both activation and silencing of the spindle checkpoint. During normal mitotic progression, checkpoint activity is sustained as long as checkpoint proteins remain on one or a few unattached kinetochores. Our results show that maintaining Mad1, specifically, on a few kinetochores is sufficient to maintain checkpoint activity. A future goal is to test whether Mad1 localization to a single kinetochore is sufficient to activate the checkpoint, which is technically challenging because we have not yet identified a stable Halo-tagged anchor protein at kinetochores that does not exchange with the cytosolic pool for the duration of the experiment (>30 minutes).

Our findings reveal two specialized properties of CENP-E at kinetochores. First, we show in live cells that CENP-E transports chromosomes from poles to the equator, whereas kinesin-1 has no directional preference. This directional transport is consistent with recent findings that a post-translational modification of tubulin, detyrosination, differentiates spindle MTs that are pointing toward the equator from astral MTs, and that CENP-E prefers detyrosinated MTs[31]. Our finding that kinesin-1 does not display a similar preference for spindle microtubules is consistent with in vitro findings that kinesin-1 is slightly less processive on detyrosinated MTs[32], although conflicting results have also been reported in neurons[33–35].

Thus, CENP-E specifically recognizes a MT code to guide chromosome congression. Second, we show that CENP-E stabilizes metaphase alignment. Given previous findings that CENP-E tracks dynamic MT tips in vitro[26], our results in vivo indicate that CENP-E acts as a tether that can prevent kinesin-1 from walking kinetochores off the end of the MT and disrupting the metaphase configuration. Many chromosomes remain aligned after depletion or inhibition of CENP-E[25,26,36], likely because other MT binding proteins at kinetochores can maintain MT attachment. Our results indicate that kinetochores lacking CENP-E are more vulnerable to perturbations, however, such as those introduced by our kinesin-1 recruitment. Overall, our results support a two-step model in which CENP-E transports kinetochores to MT plus-ends during congression and then maintains attachment of bi-oriented sister kinetochores to MT ends during metaphase oscillations.

This work establishes a foundation for optogenetic control of kinetochore function and highlights the advantages of a hybrid chemical and genetic approach. We are able to manipulate both gain and loss of enzymatic activities using light, with flexibility provided by the choice of proteins to tag and the choice of probes. We envision our approach to be readily adapted to probe other kinetochore processes, such as regulation by kinases and phosphatases, tension sensing and MT capture[37–39]. Our optogenetic tools are also broadly applicable to experimentally probe other dynamic cellular processes that depend on spatiotemporal regulation of protein localization.

Online Methods

Dimerizer synthesis, characterization and storage

Details of dimerizer synthesis and characterization with NMR spectra are in supplementary information. Dimerizers were dissolved in DMSO at 10 mM and stored in amber plastic microcentrifuge tubes at −80 °C for long-term storage. For experiments, an aliquot was diluted in cell culture medium to final working concentration and kept at −20 °C, then warmed to 37 °C when ready to use. Care was taken to minimize exposure of dimerizers to light and heat prior to experiments. Working quickly in normal room lighting, or low levels of white light used for differential interference contrast microscopy, did not cause detectable premature cleavage of TNH or uncaging of CTH.

Plasmids

All plasmids in this study are derived from pEM705, which contains a CAG promoter for constitutive expression, obtained from E. V. Makeyev[40]. Plasmid 764: Halo-GFP-ActA includes the C-terminal 47 amino acids of the *Listeria monocytogenes* ActA gene, which confer mitochondrial outer membrane targeting. Plasmid 775: PEX3-GFP-Halo includes the N-terminal 42 amino acids of the human Pex3 gene, which confer peroxisome targeting. Plasmid 767: KLC1-mCherry-eDHFR includes residues 1–175 of rat kinesin-1 light chain. Plasmid 768: K560-mCherry-eDHFR includes residues 1–560 of human kinesin-1 heavy chain. Plasmid 770: BICD-mCherry-eDHFR includes residues 1–572 of mouse BICD2. Plasmids 764, 767, 768, 770, and 775 were previously reported[41, 42]. Plasmid 850: Halo-GFP-CENP-T contains the full length human kinetochore protein CENP-T. Plasmid 858: 3xHalo-GFP-SPC25 has three Haloenzymes fused to full length human kinetochore protein

SPC25. Plasmid 841: mCherry-eDHFR-Mad1 was made by inserting Mad1 into plasmid 752: mCherry-eDHFR. CENP-E^{620} and CENP-E^{467} are truncations of human CENP-E (amino acids 1–620 or 1–467), which based on sequence contain the motor domain and a short part of the coiled-coil region but lack a significant part of the stalk, the kinetochore binding domain, and the second MT binding site[43,44]. CENP-E^{467}-mCherry-eDHFR and CENP-E^{620}-mCherry-eDHFR were derived from plasmid 768: K560-mCherry-eDHFR. The CENP-E^{620} cDNA with nucleotide sequence optimized for *E. coli* was amplified using PCR to generate CENP-E^{620} and CENP-E^{467}.

Cell culture and cell lines

All experiments were performed with HeLa acceptor cells as previously described[41], originally obtained from E.V. Makayev, Nanyang Technological University, Singapore[40]. Cells were cultured in growth medium (Dulbecco's Modified Eagle's medium with 10% FBS and 1% penicillin–streptomycin) at 37 °C in a humidified atmosphere with 5% CO_2. The cell line stably expressing Haloenzyme fused to CENP-B in Supplemental Figure 1a was reported previously[41]. All kinetochore experiments were performed with Haloenzyme tagged kinetochore proteins (Mis12, SPC25 and CENP-T) stably expressed in cell lines. The eDHFR constructs (Mad1 or motor proteins) were transiently expressed by transfection with Lipofectamine 2000 (Invitrogen) 24 hours prior to imaging, following the manufacturer's protocol. Transfections for Figure 1 and Supplementary Figure 1 were with a ratio of 1 μg plasmid DNA to 6 uL of Fugene 6 (Promega) 40 hours prior to the experiment. The Mis12-GFP-Halo cell line was created using CRISPR-Cas 9 to tag the endogenous Mis12 with Haloenzyme and GFP[45], and GFP-positive cells were sorted with flow cytometry. Guide RNAs used for Mis12 are CACCGTTAATTGCTCAGTAGTCAAA and AAACTTTGACTACTGAGCAATTAAC. Halo-GFP-CENP-T and Halo-GFP-SPC25 cell lines were created using the HILO recombinase-mediated cassette exchange system (obtained from E.V. Makeyev, Nanyang Technological University, Singapore)[40]. Briefly, Hela acceptor cells at 60–80% confluency in a well of a 6-well plate were transfected with 1 μg of Halo-GFP-SPC25 or Halo-GFP-CENP-T plasmid together with 10 ng of a Cre recombinase plasmid using Lipofectamine 2000. Two days after transfection, 1 μg/mL puromycin was added to the growth medium to select stable cell lines. After selection, the top 5% of Halo-GFP-SPC25 positive cells were sorted and collected with flow cytometry. For CENP-E siRNA, cells were cotransfected with CENP-E siRNA[7] together with either K560-1–mCherry–eDHFR, CENP-E^{46}–mCherry–EDHFR, or CENP-E^{620}–mCherry–EDHFR. Cells at ~60–80% confluency in one well of a 6-well plate were transfected with 1 μg of plasmid DNA and 2 μg of siRNA using 5 μL Lipofectamine 2000. Experiments were performed 24–48 h after transfection.

Dimerizer cytotoxicity assay

AlamarBlue (Molecular ProbesTM, catalog no. DAL1100) cell viability assays were performed following the protocol provided by the manufacturer (ThermoFisher Scientific). The assay is based on conversion of a water-soluble dye, Resazurin, into a fluorescent and colorimetric indicator by metabolically active cells. Damaged and non-viable cells generate lower signal due to reduced metabolic activity. HeLa cells expressing Halo-GFP-Spc25 were cultured in a 96-well assay plate (Corning Incorporated Costar 3603), ~1×10^4 cells per well.

Cells were treated with CTH or TNH, or with DMSO or Blasticidin S HCl (10 μg/mL, ThermoFisher Scientific catalog no. A1113903) as controls. The final DMSO concentration was kept at 0.5% in 100 μL media in each well. After incubating with the dimerizers for 24 h, cells were washed once with 200 μL of fresh DMEM, then incubated with the AlamarBlue reagent (10X dilution in DMEM medium) for 2 h to allow conversion of resazurin to resorufin. The fluorescence signal was measured at 37°C with 550 nm excitation and 590 nm emission wavelengths, using a Tecan plate reader (model, Infinite® M1000 PRO) operated by Tecan i-control software. The fluorescence signal was background subtracted based on wells without cells and calculated as a percentage of the signal from DMSO control cells. Each dimerizer concentration was tested in quadruplicate, and data were averaged over three independent experiments.

Image acquisition

For live imaging, cells were seeded on 22×22mm glass coverslips (no. 1.5; Fisher Scientific) coated with poly-D-lysine (Sigma-Aldrich) in single wells of a 6-well plate. When ready for imaging, coverslips were mounted in magnetic chambers (Chamlide CM-S22-1, LCI) with cells maintained in L-15 medium without phenol red (Invitrogen) supplemented with 10% FBS and 1% penicillin/streptomycin at 37 °C on a heated stage in an environmental chamber (Incubator BL; PeCon GmbH). Images were acquired with a spinning disk confocal microscope (DM4000; Leica) with a ×100 1.4 NA objective, an XY Piezo-Z stage (Applied Scientific Instrumentation), a spinning disk (Yokogawa), an electron multiplier charge-coupled device camera (ImageEM; Hamamatsu Photonics), and a laser merge module equipped with 488- and 593-nm lasers (LMM5; Spectral Applied Research) controlled by MetaMorph software (Molecular Devices). For Mad1 experiments, time series were taken with time interval and duration manually decided based on cell cycle progression, and z-stacks for both GFP and mCherry channel were taken with 0.5 μm spacing for a total of 3 μm. For motor experiments, time series were taken with a time interval of 20 seconds for total of 10 minutes, and z-stacks for both GFP and mCherry channel were taken with 0.5 μm spacing for a total of 5 μm, or in some cases (Figure 4 and Supplementary Figure 4) 0.5–0.75 μm spacing for 15 steps. mCherry images in some cases (Figure 4 and Supplementary Figure 4) were obtained less frequently, with a time interval of 60–120 seconds.

Dimerization and photo-activation

For CTH experiments, cells were incubated with 10 μM CTH for 1h, followed by a 30 minute washout to remove unbound CTH. For TNH experiments, 100 nM TNH was added directly to cells on the microscope stage. Targeted uncaging or cleavage was performed with an iLas2 illuminator system (Roper Scientific), equipped with a 405 nm laser (CrystaLaser LC model # DL405-050-O, output of 27 mW after fiber coupling) controlled using the iLas2 software module within Metamorph. For whole-cell UV exposure experiments (Figure 1c), light from a mercury arc lamp (Osram HXP R 120W/45c Vis) was filtered through a 387/11 nm band pass filter (Semrock part #FF01-387/11 as a component in a DAPI filter cube) and focused through the objective. For targeted irradiation with the 405 nm laser, a region of interest was defined using Metamorph. 7% laser power and 20 repetitions were used for CTH activation, and 8% and 40 repetitions were used for TNH cleavage unless otherwise stated. The CENP-E inhibitor GSK923295 (Cayman Chemical Company) was used at 50

nM and added to cells together with CTH and kept in the medium during CTH washout and imaging.

Statistical analyses

Statistical analyses methods are described in figure legends.

Image processing

Images were processed with ImageJ[47]. All images shown are maximum-intensity projections from all slices in z-stacks, except for mCherry images in Figure 4, which are maximum-intensity projections of z-sections with visible mCherry to improve the signal to noise ratio. For Figures 3 and 4, kinetochore pairs were manually tracked to locate the start and end points of movement, and direction vectors were estimated by linking the start and end points. The pole-to-pole axis was defined by manually drawing a line perpendicular to the metaphase plate through the two pole regions. The spindle region was drawn manually by linking the pole and the edges of the metaphase plate. Coordinates were imported into MATLAB (MathWorks), and the angle between the direction of kinetochore movement and the pole-to-pole axis was calculated and plotted by placing the origin of movement at the origin of the coordinate plane, with the pole-to-pole axis as the horizontal axis. For quantification in Figure 5, cells of interest in the Halo-GFP-SPC25 channel were cropped out from a maximum projection image and registered using the plugin StackReg with scaled rotation. The equator was estimated by manually drawing a line through the kinetochores at the first time point. For cells with CENP-E inhibitor, a region was drawn to include kinetochores at the equator and exclude those at the poles at the first time point, and only kinetochores in this region were analyzed for the following time points. Kinetochore coordinates were obtained by finding maxima in ImageJ and imported into MATLAB to calculate the average distance to the equator at each time point. Moving averages (Figure 5d) were obtained with the smooth function in MATLAB.

Data availability

All data generated during this study are included in this article and its supplementary information file. Our research resources, including protocols, cells, and dimerizers are available upon request. The corresponding authors adhere to the NIH Grants Policy and Sharing of Unique Research Resources.

Supplementary Material

Refer to Web version on PubMed Central for supplementary material.

Acknowledgments

We thank Dr. George Furst and Dr. Jun Gu for NMR assistance, Dr. Rakesh Kohli for High Resolution Mass Spectrometry (HRMS) assistance, Dr. Abram Calderon and Mr. Alpler Gokden for assistance with molecular cloning and generating cell lines, Drs. Don Cleveland and Ekaterina Grishchuk for CENP-E plasmids, Dr. Luke Lavis for dye JF585, and Dr. Ekaterina Grishchuk and members of the Lampson lab for helpful discussions. C.A. thanks the Royal Thai Government for PhD fellowship funding through the Development and Promotion of Science and Technology (DPST) Project. This work was supported by the National Institutes of Health (GM083988 to M.A.L. and GM118510 to D.M.C.) and the National Institutes of Health, National Cancer Institute (U54-CA193417).

References

1. Nagpal H, Fukagawa T. Kinetochore assembly and function through the cell cycle. Chromosoma. 2016; 125:645–659. [PubMed: 27376724]
2. Pesenti ME, Weir JR, Musacchio A. Progress in the structural and functional characterization of kinetochores. Curr Opin Struct Biol. 2016; 37:152–163. [PubMed: 27039078]
3. Cheeseman IM. The Kinetochore. Cold Spring Harb Perspect Biol. 2014; 6:1–18.
4. Holland AJ, Cleveland DW. Losing balance: the origin and impact of aneuploidy in cancer. EMBO Rep. 2012; 13:501–14. [PubMed: 22565320]
5. Walczak CE, Cai S, Khodjakov A. Mechanisms of chromosome behaviour during mitosis. Nat Rev Mol Cell Biol. 2010; 11:91–102. [PubMed: 20068571]
6. Auckland P, McAinsh AD. Building an integrated model of chromosome congression. J Cell Sci. 2015; 128:3363–3374. [PubMed: 26330530]
7. Lara-Gonzalez P, et al. The spindle assembly checkpoint. Curr Biol. 2012; 22:R966–80. [PubMed: 23174302]
8. London N, Biggins S. Signalling dynamics in the spindle checkpoint response. Nat Rev Mol Cell Biol. 2014; 15:736–748. [PubMed: 25303117]
9. Goshima G, Vale RD. The roles of microtubule-based motor proteins in mitosis: comprehensive RNAi analysis in the Drosophila S2 cell line. J Cell Biol. 2003; 162:1003–16. [PubMed: 12975346]
10. Lampson MA, Kapoor TM. Unraveling cell division mechanisms with small-molecule inhibitors. Nat Chem Biol. 2006; 2:19–27. [PubMed: 16408087]
11. Magidson V, Lončarek J, Hergert P, Rieder CL, Khodjakov A. Laser microsurgery in the GFP era: a cell biologist's perspective. Methods Cell Biol. 2007; 82:237–266.
12. Toettcher JE, Voigt CA, Weiner OD, Lim WA. The promise of optogenetics in cell biology: interrogating molecular circuits in space and time. Nat Methods. 2011; 8:35–38. [PubMed: 21191370]
13. van Bergeijk P, Adrian M, Hoogenraad CC, Kapitein LC. Optogenetic control of organelle transport and positioning. Nature. 2015; 518:111–114. [PubMed: 25561173]
14. Jost APT, Weiner OD. Probing yeast polarity with acute, reversible, optogenetic inhibition of protein function. ACS Synth Biol. 2015; 4:1077–1085. [PubMed: 26035630]
15. Ballister ER, Aonbangkhen C, Mayo AM, Lampson Ma, Chenoweth DM. Localized light-induced protein dimerization in living cells using a photocaged dimerizer. Nat Commun. 2014; 5:5475. [PubMed: 25400104]
16. Ballister ER, Ayloo S, Chenoweth DM, Lampson Ma, Holzbaur ELF. Optogenetic control of organelle transport using a photocaged chemical inducer of dimerization. Curr Biol. 2015; 25:R407–R408. [PubMed: 25989077]
17. Klán P, et al. Photoremovable protecting groups in chemistry and biology: reaction mechanisms and efficacy. Chem Rev. 2013; 113:119–91. [PubMed: 23256727]
18. Ballister ER, Riegman M, Lampson Ma. Recruitment of Mad1 to metaphase kinetochores is sufficient to reactivate the mitotic checkpoint. J Cell Biol. 2014; 204:901–908. [PubMed: 24637323]
19. Kuijt TEF, Omerzu M, Saurin AT, Kops GJPL. Conditional targeting of MAD1 to kinetochores is sufficient to reactivate the spindle assembly checkpoint in metaphase. Chromosoma. 2014; 123:471–80. [PubMed: 24695965]
20. Kapoor TM, et al. Chromosomes can congress to the metaphase plate before biorientation. Science. 2006; 311:388–391. [PubMed: 16424343]
21. Barisic M, Aguiar P, Geley S, Maiato H. Kinetochore motors drive congression of peripheral polar chromosomes by overcoming random arm-ejection forces. Nat Cell Biol. 2014; 16:1249–1256. [PubMed: 25383660]
22. Wood KW, et al. Antitumor activity of an allosteric inhibitor of centromere-associated protein-E. Proc Natl Acad Sci U S A. 2010; 107:5839–44. [PubMed: 20167803]

23. Cooke CA, Schaar B, Yen TJ, Earnshaw WC. Localization of CENP-E in the fibrous corona and outer plate of mammalian kinetochores from prometaphase through anaphase. Chromosoma. 1997; 106:446–55. [PubMed: 9391217]
24. Shrestha RL, Draviam VM. Lateral to end-on conversion of chromosome-microtubule attachment requires kinesins CENP-E and MCAK. Curr Biol. 2013; 23:1514–26. [PubMed: 23891108]
25. Putkey FR, et al. Unstable kinetochore-microtubule capture and chromosomal instability following deletion of CENP-E. Dev Cell. 2002; 3:351–365. [PubMed: 12361599]
26. Gudimchuk N, et al. Kinetochore kinesin CENP-E is a processive bi-directional tracker of dynamic microtubule tips. Nat Cell Biol. 2013; 15:1079–88. [PubMed: 23955301]
27. Strickland D, et al. TULIPs: tunable, light-controlled interacting protein tags for cell biology. Nat Methods. 2012; 9:379–384. [PubMed: 22388287]
28. Yang X, Jost APT, Weiner OD, Tang C. A light-inducible organelle-targeting system for dynamically activating and inactivating signaling in budding yeast. Mol Biol Cell. 2013; 24:2419–30. [PubMed: 23761071]
29. Levskaya A, Weiner OD, Lim WA, Voigt CA. Spatiotemporal control of cell signalling using a light-switchable protein interaction. Nature. 2009; 461:997–1001. [PubMed: 19749742]
30. Maldonado M, Kapoor TM. Constitutive Mad1 targeting to kinetochores uncouples checkpoint signalling from chromosome biorientation. Nat Cell Biol. 2011; 13:475–482. [PubMed: 21394085]
31. Barisic M, et al. Microtubule detyrosination guides chromosomes during mitosis. Science. 2015; 348:799–803. [PubMed: 25908662]
32. Sirajuddin M, Rice LM, Vale RD. Regulation of microtubule motors by tubulin isotypes and post-translational modifications. Nat Cell Biol. 2014; 16:335–344. [PubMed: 24633327]
33. Dunn S, et al. Differential trafficking of Kif5c on tyrosinated and detyrosinated microtubules in live cells. J Cell Sci. 2008; 121:1085–1095. [PubMed: 18334549]
34. Konishi Y, Setou M. Tubulin tyrosination navigates the kinesin-1 motor domain to axons. Nat Neurosci. 2009; 12:559–567. [PubMed: 19377471]
35. Hammond JW, et al. Posttranslational modifications of tubulin and the polarized transport of kinesin-1 in neurons. Mol Biol Cell. 2010; 21:572–83. [PubMed: 20032309]
36. McEwen BF, et al. CENP-E is essential for reliable bioriented spindle attachment, but chromosome alignment can be achieved via redundant mechanisms in mammalian cells. Mol Biol Cell. 2001; 12:2776–89. [PubMed: 11553716]
37. Heald R, Khodjakov A. Thirty years of search and capture: The complex simplicity of mitotic spindle assembly. J Cell Biol. 2015; 211:1103–1111. [PubMed: 26668328]
38. Lampson M, Grishchuk E. Mechanisms to avoid and correct erroneous kinetochore-microtubule attachments. Biology (Basel). 2017; 6:1.
39. Funabiki H, Wynne DJ. Making an effective switch at the kinetochore by phosphorylation and dephosphorylation. Chromosoma. 2013; 122:135–158. [PubMed: 23512483]
40. Khandelia P, Yap K, Makeyev EV. Streamlined platform for short hairpin RNA interference and transgenesis in cultured mammalian cells. Proc Natl Acad Sci U S A. 2011; 108:12799–804. [PubMed: 21768390]
41. Ballister ER, Aonbangkhen C, Mayo AM, Lampson Ma, Chenoweth DM. Localized light-induced protein dimerization in living cells using a photocaged dimerizer. Nat Commun. 2014; 5:5475. [PubMed: 25400104]
42. Ballister ER, Ayloo S, Chenoweth DM, Lampson Ma, Holzbaur ELF. Optogenetic control of organelle transport using a photocaged chemical inducer of dimerization. Curr Biol. 2015; 25:R407–R408. [PubMed: 25989077]
43. Yen TJ, Li G, Schaar BT, Szilak I, Cleveland DW. CENP-E is a putative kinetochore motor that accumulates just before mitosis. Nature. 1992; 359:536–539. [PubMed: 1406971]
44. Liao H, Li G, Yen TJ. Mitotic regulation of microtubule cross-linking activity of CENP-E kinetochore protein. Science. 1994; 265:394–8. [PubMed: 8023161]
45. Ran FA, et al. Genome engineering using the CRISPR-Cas9 system. Nat Protoc. 2013; 8:2281–2308. [PubMed: 24157548]

46. Johnson VL, Scott MIF, Holt SV, Hussein D, Taylor SS. Bub1 is required for kinetochore localization of BubR1, Cenp-E, Cenp-F and Mad2, and chromosome congression. J Cell Sci. 2004; 117:1577–1589. [PubMed: 15020684]

47. Schneider CA, Rasband WS, Eliceiri KW. NIH Image to ImageJ: 25 years of image analysis. Nat Methods. 2012; 9:671–675. [PubMed: 22930834]

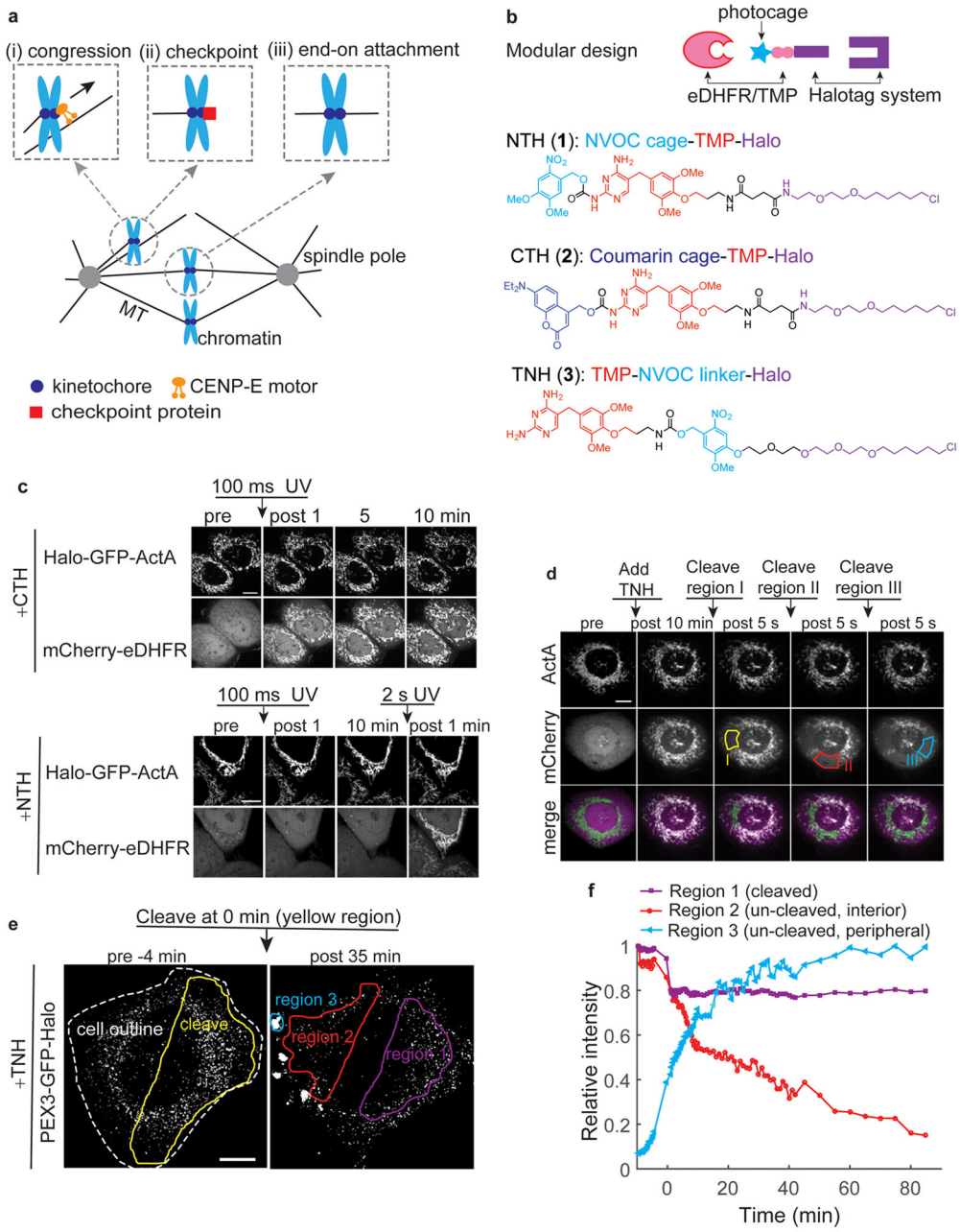

Figure 1. New dimerizers based on a modular design

(**a**) Kinetochore functions in cell division. (i) Chromosome congression: CENP-E motors at kinetochores transport chromosomes to the spindle equator. (ii) Checkpoint signaling proteins localize to unattached kinetochores. (iii) Bi-oriented kinetochores maintain stable end-on MT attachment. (**b**) Optogenetic toolbox: NTH was previously published[15]; CTH uses a different photocage; TNH is photocleavable between TMP and Halo. (**c**) Cells expressing mCherry-eDHFR and Halo-GFP-ActA, which localizes to mitochondria, were incubated with 10 μM CTH or 10 μM NTH. Cells were illuminated with a 100 ms pulse of wide field UV (387±5 nm), which was sufficient to uncage CTH but not NTH, followed by a

2 sec pulse to uncage NTH. (**d**) Cells expressing mCherry-eDHFR and Halo-GFP-ActA were incubated with 100 nM TNH to recruit mCherry to mitochondria. Three regions were illuminated sequentially with a 405 nm laser to cleave TNH and release mCherry from Mitochondria. (**e, f**) Cells expressing KLC1-mCherry-eDHFR and PEX3-GFP-Halo, which localizes to peroxisomes, were treated with 100 nM TNH at t=−4 min to induce peroxisome transport towards the cell periphery. Half the cell (yellow region) was illuminated with a 405 nm laser at t=0 to cleave TNH. GFP intensity was quantified (f) in the interior region (1) where TNH was cleaved and in interior and peripheral regions (2 and 3 respectively) that were not exposed to 405 nm light. Intensity in each region over time is shown as a fraction of the maximal intensity in that region. Scale bars 10 μm.

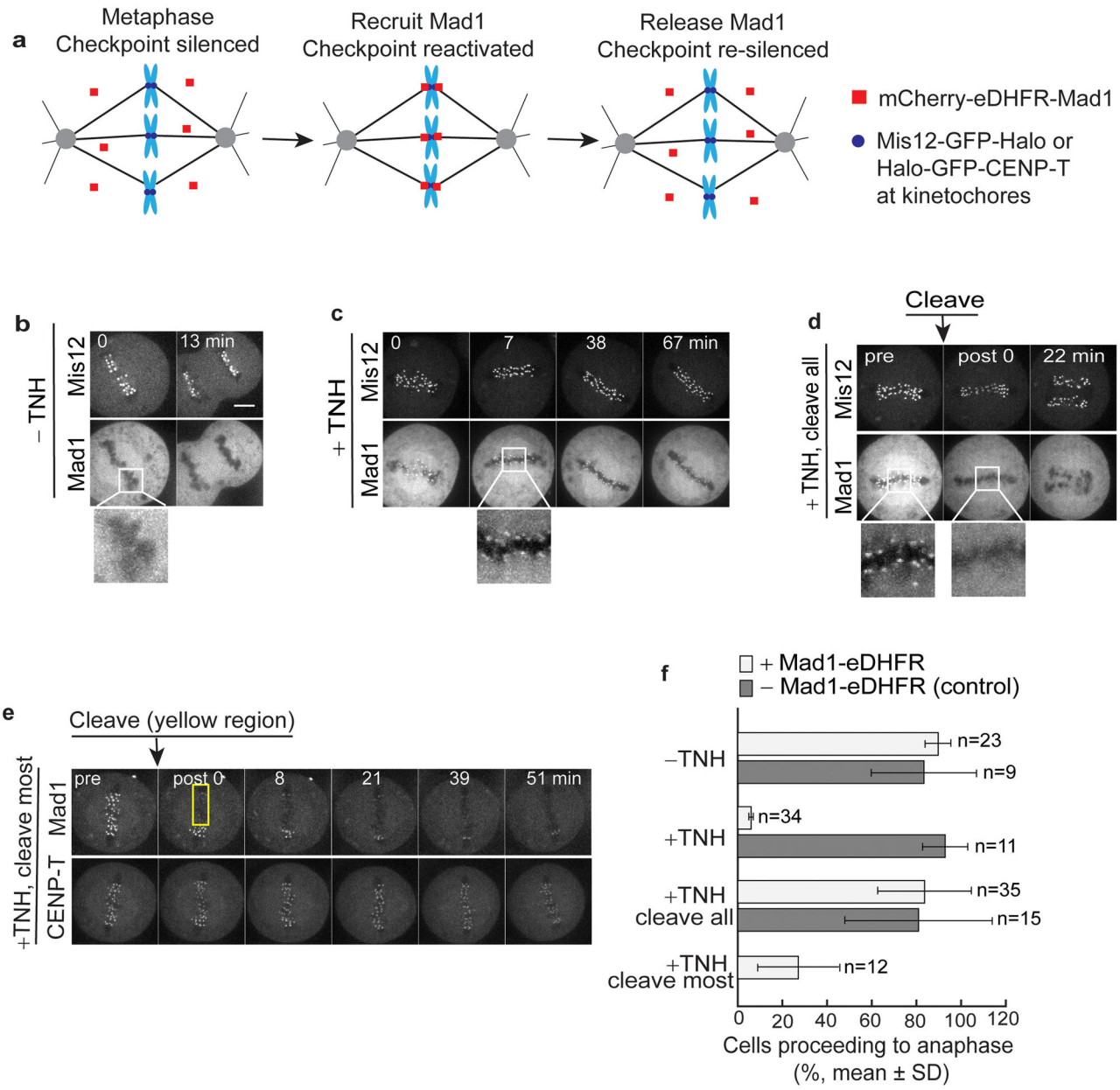

Figure 2. Activating and silencing the spindle checkpoint

(**a**) Experimental design for cells expressing mCherry-eDHFR-Mad1 and either Mis12-GFP-Halo or Halo-GFP-CENP-T. (**b**) Control experiment: with no TNH and no Mad1 recruitment to metaphase kinetochores, cells proceeded to anaphase normally. (**c–f**) With 100 nM TNH, eDHFR-Mad1 was recruited to metaphase kinetochores. Without cleavage (c) cells arrested in metaphase. TNH cleavage over the whole cell at t=0 released Mad1 from all kinetochores (d), and cells proceeded to anaphase. TNH cleavage in a region covering most of the metaphase plate (e, yellow rectangle) released Mad1 from kinetochores in this region, and cells arrested in metaphase. The percentage of cells entering anaphase within 30 minutes

under the indicated conditions was quantified (f) for cells with or without eDHFR-Mad1. Error bars are standard deviation from three experiments. Scale bars 5 μm.

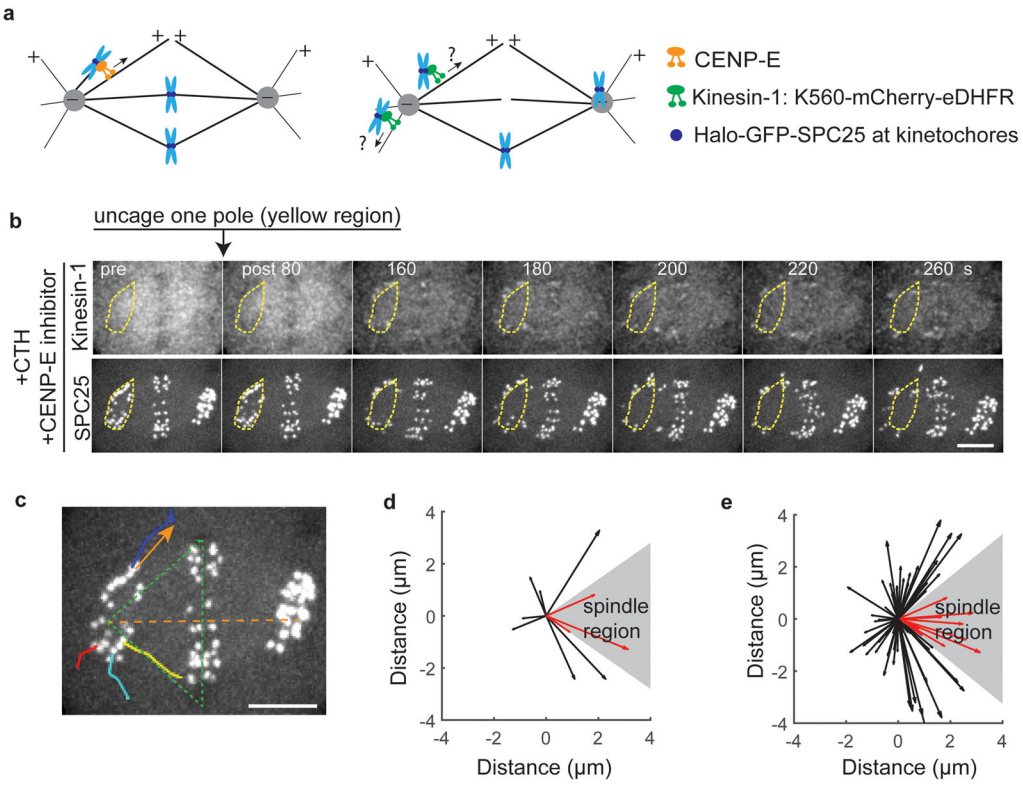

Figure 3. Kinesin-1 transports chromosomes in all directions from the pole

(**a**) Model for CENP-E transporting pole-proximal chromosomes specifically toward the equator (left) and experimental design (right) to test whether kinesin-1, another plus-end directed motor, can rescue CENP-E inhibition in cells expressing Halo-GFP-SPC25 and K560-mCherry-eDHFR (kinesin-1). (**b–e**) Cells were treated with the CENP-E inhibitor GSK923295 and with CTH, then CTH was uncaged at one pole (b, yellow region) to recruit kinesin-1 motors to kinetochores at that pole, and cells were imaged live for 10 minutes. Solid lines (c) are representative trajectories of kinetochore movements for the cell shown in (b). For each kinetochore, a direction vector was estimated by linking the start and end points (e.g., orange arrow). The pole-pole axis (orange dashed line) and the spindle region (dashed green triangle) were drawn manually. Direction vectors are plotted for kinetochore movements at the uncaged pole in a single cell, (d, corresponding to cell shown in b and c), and for multiple cells (e, n=75 kinetochore pairs from 9 cells). The pole-pole axis is the horizontal axis, and starting points for each kinetochore are superimposed at the origin. Red arrows represent movement towards the metaphase plate. Scale bars 5 μm.

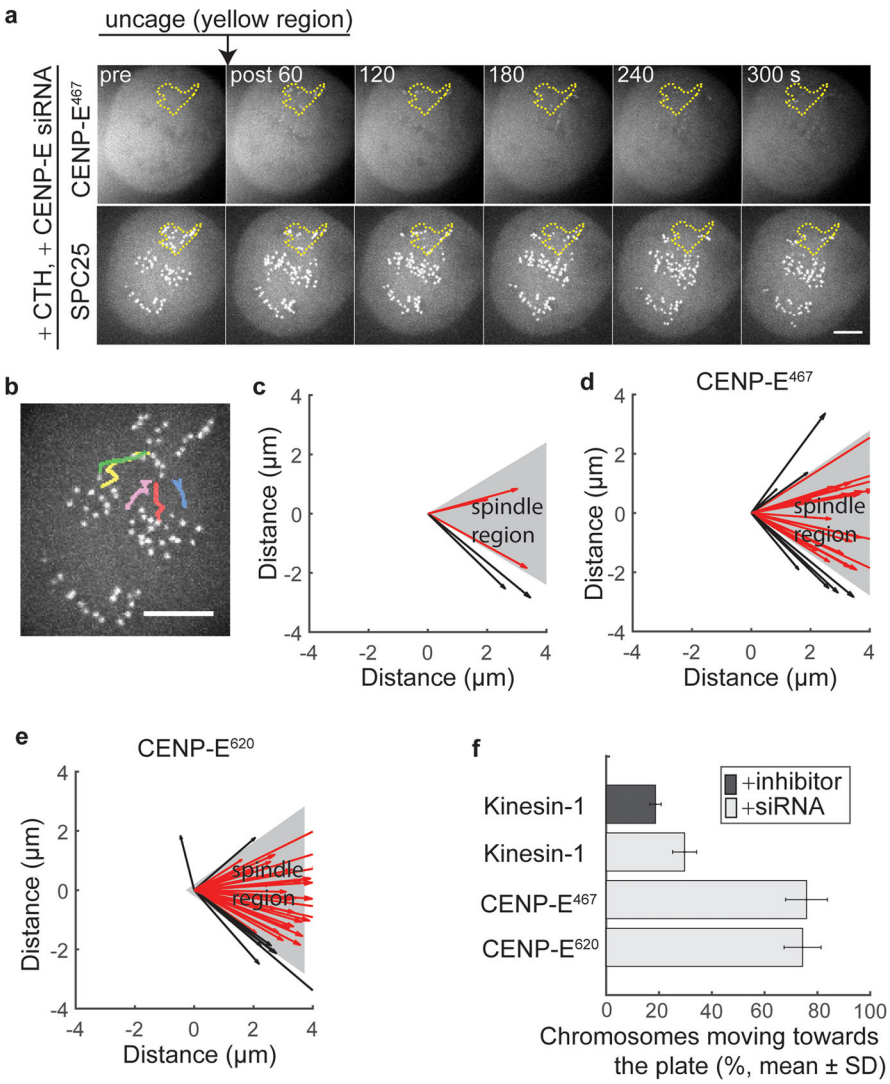

Figure 4. CENP-E transports chromosomes from the pole to the equator

(**a–e**) Cells expressing Halo-GFP-SPC25 and CENP-E^{467}-mCherry-eDHFR (a–d) or CENP-E^{620}-mCherry-eDHFR (e) were treated with CENP-E siRNA and CTH. CTH was uncaged at one pole (yellow region), and cells were imaged live for 10 minutes. Solid lines (b) are representative trajectories of kinetochore movements for the cell shown in (a). Direction vectors are plotted as in Figure 3 for kinetochore movements at the uncaged pole in a single cell (c, corresponding to cell shown in a and b) and for multiple cells (d, n=29 kinetochore pairs from 12 cells, e, n=39 kinetochores pairs from 14 cells). Scale bars 5 μm. **(f)** Percent of chromosomes moving towards the metaphase plate after recruitment of kinesin-1 or CENP-E, with endogenous CENP-E inhibited either with the inhibitor GSK923295 or by siRNA.

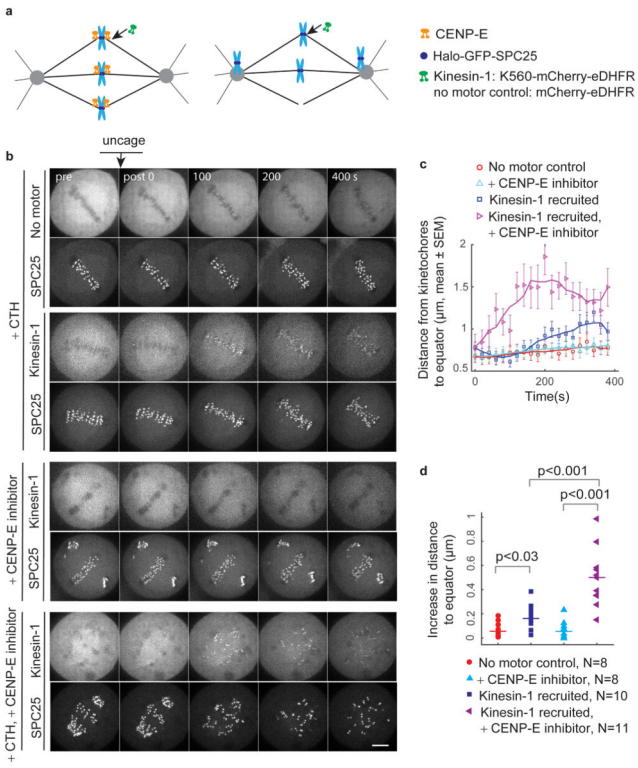

Figure 5. CENP-E stabilizes metaphase alignment

(**a**) Experimental design to test whether CENP-E is necessary to maintain metaphase alignment by recruiting kinesin-1 motors to kinetochores in cells expressing Halo-GFP-SPC25 and K560-mCherry-eDHFR (kinesin-1), with (right) or without (left) CENP-E inhibited. (**b–d**) Cells were treated with CTH and/or CENP-E inhibitor as indicated. CTH was uncaged at t=0 to recruit K560-mCherry-eDHFR (or mCherry-eDHFR as a control) to all kinetochores. Cells were treated with. Mean distances of kinetochores to the equator over time are plotted for single cells (c, corresponds to cells shown in b), with moving averages shown as solid lines (n>16 kinetochores, error bars SEM). To compare data from multiple cells (d), mean distance was averaged over the 300 to 400 second time window, and the mean distance at t=0 was subtracted. Each data point represents a single cell; horizontal line, mean. P values are from two-sided t-test. Scale bar 5 µm.